

RSC Advances



This is an *Accepted Manuscript*, which has been through the Royal Society of Chemistry peer review process and has been accepted for publication.

Accepted Manuscripts are published online shortly after acceptance, before technical editing, formatting and proof reading. Using this free service, authors can make their results available to the community, in citable form, before we publish the edited article. This *Accepted Manuscript* will be replaced by the edited, formatted and paginated article as soon as this is available.

You can find more information about *Accepted Manuscripts* in the [Information for Authors](#).

Please note that technical editing may introduce minor changes to the text and/or graphics, which may alter content. The journal's standard [Terms & Conditions](#) and the [Ethical guidelines](#) still apply. In no event shall the Royal Society of Chemistry be held responsible for any errors or omissions in this *Accepted Manuscript* or any consequences arising from the use of any information it contains.

Two Physical Strategies to Reinforce Nonmetallic Photocatalyst, $g\text{-C}_3\text{N}_4$: Vacuum Heating and Electron Beam Irradiation

Yunlong Zhang, Haijiao Zhang, Lingli Cheng, Yujia Wang, Yu Miao, Guoji Ding, and Zheng Jiao*

School of Environmental and Chemical Engineering, Shanghai University, Shanghai, P. R. China

* E-mail: zjiao@shu.edu.cn; Homepage: www.zjiao.shu.edu.cn

Keywords: Graphitic carbon nitride / $g\text{-C}_3\text{N}_4$ / Vacuum heating / Electron beam irradiation / Photocatalyst

Here we demonstrated two physical strategies, vacuum heating and electron beam irradiation, to reinforce nonmetallic photocatalyst, $g\text{-C}_3\text{N}_4$. These two post-treatments also improved the visible light absorption properties of $g\text{-C}_3\text{N}_4$, nevertheless, electron beam irradiation was more destructive, which caused a decided change for its chemical bonds and band structure. According to the post-processing parameters of this article vacuum heating (38 ± 2 mTorr for 4 days at 200°C) could enhance the photocatalytic efficiency of original $g\text{-C}_3\text{N}_4$ 2.5 times, and electron beam irradiation (760 kGy at 1.8 MeV and 8 mA·s⁻¹) could ameliorate that 4.5 times. Finally, the post-treated photocatalysts were stable during the photocatalytic oxidation and ensured those applications.

Introduction

Recently, a nonmetallic photocatalyst, graphitic carbon nitride ($g\text{-C}_3\text{N}_4$), only composed of C and N elements, drew a world-wide attention due to its potential application in solar energy conversion, photo-synthesis, electro-catalysis, and bio-imaging because of the appropriate bandgap, large surface area, and excellent chemical stability.¹⁻⁷ However, the efficiency of pure $g\text{-C}_3\text{N}_4$ was still far from satisfaction owing to the high recombination rate of photoinduced electron-hole pairs.⁸⁻¹¹ To ameliorate this disadvantage, many strategies was adopted,^{12,13} for example, metal loading (Ag,¹⁴ Pd,¹⁵ Au¹⁶), metal doping (Fe,¹⁷ Zn,¹⁸ Er¹⁹), non-metal doping (B,²⁰ O,²¹ S²²), morphological control (Nanotubes,²³ Nanorods,²⁴ Quantum Dots²⁵), compositing support (GO,²⁶ CNT,²⁷ SBA-15²⁸) and coupling with other semiconductors (S₈,²⁹ Ag₃PO₄,³⁰ SrTiO₃,³¹ Bi₂WO₆,³² ZnO,³³ MoS₂,³⁴ etc.).³⁵ Nonetheless, the majority of doping and composite attempts inevitably need to introduce some other substances.

In our past work, we demonstrated a vacuum heating treatment with low and easily achievable degree of vacuum to improve the photocatalytic properties of TiO₂.³⁶ Vacuum heating³⁷ as well as hydrogenation³⁸ could alter the surface structure of TiO₂ to enhance the optical absorption region. On the other hand, the radiation-induced effects in the TiO₂ crystal structure, especially electron beam irradiation, was reported.^{39,40} The band gap of TiO₂ was decreased after electron beam irradiation without using any dopants.

Herein, we introduced, for the first time, the vacuum heating and electron beam irradiation post-treatments into strengthening of nonmetallic photocatalyst, $g\text{-C}_3\text{N}_4$. The $g\text{-C}_3\text{N}_4$ photocatalysts after vacuum heating or electron beam irradiation were characterized by XRD, FT-IR, Raman, UV-Vis DRS, PL and XPS analysis. The photodegradation of RhB was employed to evaluate the photocatalytic activities under visible light irradiation, and the stability of the synthesized photocatalysts was also investigated

through four successive experimental runs. Moreover, we compared the similarities and differences of the results caused by these two treatments.

Results and Discussion

Typical $g\text{-C}_3\text{N}_4$ was synthesized by thermal treatment of urea under ambient pressure in air directly.⁴¹ In brief, 4.0 g of urea was transferred into a 25 mL of crucible with a cover, and the crucible was heated in a muffle furnace at 80°C (24 h) for drying and 550°C (3 h) for thermal reaction (ramp rate of $5^\circ\text{C}\cdot\text{min}^{-1}$ from 80°C to 550°C), and then air-cooled to the room temperature. Finally, the yellow-colored product was washed with nitric acid (0.1 mol·L⁻¹) and water several times, and dried at 60°C overnight.

Vacuum heating: the resulting $g\text{-C}_3\text{N}_4$ was treated under vacuum of 38 ± 2 mTorr for 2 (or 4) days at 200°C . A degasser (FloVac; Quantachrome) applied to detect and control the vacuum which was provided by a rotary vane vacuum pump (Duo 3, Pfeiffer Vacuum).

Electron beam irradiation: a mixture which contained 60 mg of obtained $g\text{-C}_3\text{N}_4$, 30 mg of water, 3 ml of isopropanol and 60 μL of ammonium hydroxide was sealed in a polythene bag (10 cm \times 15 cm \times 5 mm), and the bag was irradiated under a dynamiron (GJ-2-L, Shanghai Xianfeng Motor Factory Co., Ltd.) with an accelerating voltage of 1.8 MeV and an accelerating current of 8 mA·s⁻¹ at room temperature. The irradiation dose was set at 380 (or 760) kGy.

We labelled these samples after different treatments with CN-VA- (or CN-EB-) as prefix followed by the vacuum heating time (or the EB irradiation dose). For instance, CN-VA-4 indicated that the $g\text{-C}_3\text{N}_4$ was subjected to vacuum heating for 4 days, and CN-EB-380 denoted that the $g\text{-C}_3\text{N}_4$ underwent electron beam irradiation with a dose of 380 kGy. In addition, CN suggested an original $g\text{-C}_3\text{N}_4$ without any post-processing.

By way of thermal polymerization of urea directly, the typical graphitic carbon nitride was synthesized, as shown in **Fig. 1**. The TEM image presented a two-dimensional sheet structure with

irregular wrinkles, furthermore, a number of pores distributed over its surface according to the corresponding SEM image. The nitrogen adsorption-desorption isotherm and Barrett-Joyner-Halenda (BJH) pore size distribution curve (**Fig. S1**) indicated that $g\text{-C}_3\text{N}_4$ exhibited type IV isotherm with H3 hysteresis loop. The Brunauer-Emmett-Teller (BET) specific surface area was calculated to be $150.4\text{ m}^2\text{ g}^{-1}$, higher than previous report,⁴¹ which would lead to the more efficient surface adsorption and faster photogenerated carrier separation, and then to the improvement of photoactivity.

The original $g\text{-C}_3\text{N}_4$ appeared pale-yellow (**Fig. 2a**). After vacuum heating or electron beam irradiation, the samples become darker in color, however, the color variation by the second treatment was more obvious. Although the color changed, these two treatments did not produce significant changes in the morphology (**Fig. S2**). **Fig. 3** illustrated the XRD patterns of $g\text{-C}_3\text{N}_4$ with different post-treatments. The strongest peak at 27.7° was a characteristic interlayer stacking peak of aromatic systems, indexed as the (002) plane for graphitic materials.^{20,42} The calculated interplanar distance of aromatic units was $d = 0.322\text{ nm}$. The small-angle peak at 12.8° corresponded to a distance $d = 0.692\text{ nm}$ which indexed as (100) plane and associated with an in-plane structural packing motif.^{20,42} In addition, the other two weaker peaks at 17.6 and 21.7° caused by (011) and (110) plane reflection.⁴³ It's worth noting that the (002) peak intensities of post-treated $g\text{-C}_3\text{N}_4$ decreased so that vacuum heating as well as high-energy electron beam irradiation would partly damage the fine structure of $g\text{-C}_3\text{N}_4$ and reduce its crystallinity.³⁶

In **Fig. 4a**, the FT-IR spectra revealed the original $g\text{-C}_3\text{N}_4$ chemical structure remained mostly unchanged after vacuum heating or electron beam irradiation. The absorption bands at 1573 and 1637 cm^{-1} were attributed to C=N stretching, while the four bands at 1240 , 1317 , 1403 and 1460 cm^{-1} corresponded to aromatic C-N stretching.⁴⁴⁻⁴⁶ The band at 812 cm^{-1} was assigned to the breathing vibrational modes of *s*-triazine units.⁴⁴⁻⁴⁶ The broad band at 3000 to 3700 cm^{-1} belonged to the N-H vibration due to partial condensation and the adsorbed water molecules. In the Raman spectra presented in **Fig. 4b**, all samples exhibited three bands at 707 , 769 and 975 cm^{-1} . The 769 cm^{-1} band was attributed to the out-of-plane bending mode of graphitic domains, and the rest two bands arose from the breathing modes of *s*-triazine rings.⁴⁷⁻⁴⁹ It's noteworthy that both of vacuum heating and electron beam irradiation increased the background fluorescence intensity of corresponding samples so that the relative intensity of the Raman bands was decreased, which was consistent with previous reports.^{36,37} The greater the degree of processing, the more attenuated the band intensity.

As can be seen in **Fig. 5a**, the optical properties of above-mentioned $g\text{-C}_3\text{N}_4$ samples were measured by UV-Vis DR spectra. The absorption edge of post-treated $g\text{-C}_3\text{N}_4$ displayed a trifling red shift in comparison with original $g\text{-C}_3\text{N}_4$. The corresponding band gaps of CN, CN-VA-2, CN-VA-4, CN-EB-380

and CN-EB-760 were about 2.95 , 2.94 , 2.93 , 2.97 and 2.97 eV , respectively (**Fig. 5b**). Vacuum heating resulted in a reduction in the band gap of corresponding samples, however, electron beam irradiation brought about a change in the inflection point position of absorption curve, leading to the slight decrease of calculated band gaps. In addition, the post-treated $g\text{-C}_3\text{N}_4$ exhibited more intense absorption in visible range, which was in agreement with the color change from yellow to dark yellow. This prominent optical property might be due to the broadening of band-tail, profiting from efficient light harvesting.

Fig. 5c demonstrated the PL spectra of the as-synthesized photocatalysts excited by 367 nm at room temperature. For these five samples, the main emission peak appeared at about 437 nm , which was assigned to the band-band PL phenomenon with the energy of light approximately equal to the band-gap energy.^{20,47} It's widely accepted that the enhancement of photocatalytic activity was attributed to the efficient photogenerated electron-hole pair separation.^{21,50} Obviously, in comparison with original $g\text{-C}_3\text{N}_4$, the intensity of the PL signal for CN-VA-2 and CN-VA-4 was somewhat lower, and that of CN-EB-380 and CN-EB-760 was significantly lower (also see **Fig. 2b**), which indicated that the recombination of electron-hole pairs might be effectively inhibited on the post-treated $g\text{-C}_3\text{N}_4$, especially the electron beam irradiation treatment.

XPS was undertaken to accurately determine the chemical composition and specific electronic states of the different $g\text{-C}_3\text{N}_4$ samples. In the survey spectra of all five samples (**Fig. 6a**), the typical C 1s and N 1s peaks were observed, and a residual O 1s peak probably due to calcination in air, was also present.^{45,51} **Fig. 6b** illustrated two major C 1s peaks centering at 288.5 and 289.7 eV , corresponding to sp^2 -bonded carbon (C-N-C) and C-O respectively and another trace amount of C-C bonding at 284.8 eV .^{21,41} In the high-resolution XPS spectra of N 1s, three deconvolution peaks at 399.0 , 400.3 and 401.5 eV should be ascribed to sp^2 C-N-C, sp^3 N-[C]₃, and C-NH_x (amino functional groups), respectively.^{21,41} The weak 404.5 eV peak was attributed to the π -excitations. The N 1s bonding ratios of $g\text{-C}_3\text{N}_4$ samples after different treatments were listed in **Table I**. Vacuum heating did not make the proportions of three N 1s bonds change notably, but electron beam irradiation might break the portion of C-N-C structure or convert it to N-[C]₃ structure. That was to say, the partial tri-*s*-triazine structure of $g\text{-C}_3\text{N}_4$ could be rearranged or formed to *s*-triazine structure under the electron beam irradiation. These $g\text{-C}_3\text{N}_4$ based on the two structures were allotropes, but the *s*-triazine in theoretical calculation was a metastable state.⁵² These tiny structural distortions would lead to the size reduction of the nitrogen hole in the topological arrangement of aromatic systems and cause the original flat surface to be curved in arch. The electronic energy state distributions of these raised positions were different from other locations, easy to form the separation point of photogenerated electrons and holes, which would

also cause a sharp decrease in the fluorescence effect above (Fig. 5c).

In addition, the valence band maximum (VBM) of samples (Fig. 6b) also manifested the different results led by the two post-treatments.^{21,22,53} Vacuum heating rose the position of VBM a trifle, nevertheless, electron beam irradiation reduced it observably. In comparison, vacuum heating was a relatively mild post-treatment, in previous reports,^{36,37} which mainly could produce some amorphous layer and not lead to the chemical structure or band position alteration dramatically. On the other hand, electron beam irradiation was a more destructive post-treatment, which could trigger a series of radiation chemical reactions, simultaneously including the electron beam bombardment to the material directly. With this article, electron beam irradiation not only modified the optical properties of samples but also caused a decided change for its chemical bonds and band structure.

The photocatalytic activities of different $g\text{-C}_3\text{N}_4$ samples were evaluated by the photodegradation of Rhodamine B, a probe molecule, under visible light irradiation. All of photodegradation curves were consistent with pseudo-first-order kinetic reactions (Fig. 7a). Compared to the original $g\text{-C}_3\text{N}_4$, the post-treated $g\text{-C}_3\text{N}_4$ samples exhibited more excellent photocatalytic performance, among them, the photocatalytic property of CN-VA-4 was about 2.5 times higher than that of CN and the efficiency of CN-EB-760 was about 4.5 times higher than that of CN. The greater the degree of treatment, the more remarkable the resulting upgrade. To test the stability and reusability of $g\text{-C}_3\text{N}_4$ after vacuum heating or electron beam irradiation, the CN-VA-4 and CN-EB-760 were reused for photocatalytic reaction four times under the same conditions, and the results were shown in Fig. 7b,c. The photocatalytic effects of the used samples after four photocatalytic degradation cycles were little depressed, which indicated those photocatalysts were stable during the photocatalytic oxidation of the pollutant molecules and ensured those applications.

Conclusions

In summary, we successfully introduced, for the first time, the vacuum heating and electron beam irradiation post-treatments into strengthening of nonmetallic photocatalyst, $g\text{-C}_3\text{N}_4$. These two post-treatments also improved the light absorption properties of $g\text{-C}_3\text{N}_4$, especially in the visible region. Vacuum heating was a relatively mild post-treatment, nevertheless, electron beam irradiation was more destructive, which caused a decided change for its chemical bonds and band structure. According to the post-processing parameters of this article, vacuum heating (38 ± 2 mTorr for 4 days at 200°C) could enhance the photocatalytic efficiency of original $g\text{-C}_3\text{N}_4$ 2.5 times, and electron beam irradiation (760 kGy at 1.8 MeV and $8\text{ mA}\cdot\text{s}^{-1}$) could ameliorate that 4.5 times. Finally, the post-treated photocatalysts were stable during the photocatalytic oxidation and ensured those applications.

Experimental Section

Chemicals.

Urea (NH_2ONH_2), ethanol ($\text{CH}_3\text{CH}_2\text{OH}$), nitric acid (HNO_3 , $\geq 65\%$), isopropanol ($(\text{CH}_3)_2\text{CHOH}$) and ammonium hydroxide (NH_4OH , $> 25\%$) were of analytical grade and purchased from Sinopharm Chemical Reagent Co., Ltd. (Shanghai, China). Deionized water was used throughout this study.

Photocatalysis.

The photocatalytic performance was measured by analyzing the degradation of Rhodamine B ($\text{C}_{28}\text{H}_{31}\text{ClN}_2\text{O}_3$, $\geq 95\%$, RhB, Sigma) under visible light irradiation after adding the photocatalysts (20 mg) into a RhB solution (50 mL, $20\text{ mg}\cdot\text{L}^{-1}$) with continuous air bubbles. Prior to irradiation, the suspension was bubbled for 90 min in the dark to reach an adsorption equilibrium. A 350 W Xe lamp through a UV cut-off filter (420 nm) was used as the light source. The degradation of the dye was monitored by taking 3 mL of aliquots at regular irradiation time intervals. After filtering by $0.22\ \mu\text{m}$ microporous membrane, the obtained supernatants were collected, and the concentration of RhB calculated by measuring the characteristic absorption peak of 550 nm recorded by a UV-Vis spectrophotometer (U-3010, Hitachi).

Characterization.

The morphology of the $g\text{-C}_3\text{N}_4$ was observed using a transmission electron microscope (TEM, JEM-200CX, JEOL) with an accelerating voltage of 120 kV and a field emission scanning electron microscope (FESEM, JSM-6700F, JEOL) with an accelerating voltage of 15 kV. Powder X-ray diffraction (XRD, D/max-2550, Rigaku) was employed to determine the crystalline phase of the samples, which deployed Cu $K\alpha$ radiation ($\lambda = 1.5418\ \text{\AA}$) with 40 kV and 250 mA as accelerating voltage and current respectively. The Raman spectra were obtained at room temperature on a Raman microscope (inVia plus, Renishaw) and the excitation light was the 785 nm line of a laser diode. Nitrogen sorption isotherms were measured at 77K using a surface area and pore size analyzer (Quadrastorb SI, Quantachrome). All of the samples were degassed under vacuum at 80°C overnight prior to measurement. The Fourier transform infrared (FT-IR) spectra were performed on a FT-IR spectrometer (Avatar 370, Nicolet) in the mid infrared range (4000 to 400 cm^{-1}) for samples dispersed in KBr pellets. The diffuse reflectance (DR) spectra of the photocatalysts were collected at room temperature on a UV-Vis spectrophotometer (U-3010, Hitachi) with an integrating sphere accessory and BaSO₄ as the reference. The photoluminescence (PL) spectra of the materials were acquired on a fluorescence spectrophotometer (F-7000, Hitachi) at an excitation wavelength of 367 nm. The surface chemical bonding and valence band spectra of the samples were obtained with an X-ray photoelectron spectrometer (XPS, ESCALAB 250Xi, Thermo

Scientific) equipped with an Al anode X-ray source with $K\alpha$ radiation. The position of the peaks was calibrated to the C–C 1s peak at 284.8 eV.

Acknowledgments

This work was financially supported by the National Natural Science Foundation of China (Grant No. 11275121, 21471096, 61174011 and 21371116).

References

- 1 Y. Zhao, Z. Liu, W. Chu, L. Song, Z. Zhang, D. Yu, Y. Tian, S. Xie and L. Sun, *Adv. Mater.*, 2008, **20**, 1777.
- 2 X. Wang, K. Maeda, X. Chen, K. Takanebe, K. Domen, Y. Hou, X. Fu and M. Antonietti, *J. Am. Chem. Soc.*, 2009, **131**, 1680.
- 3 X. Wang, K. Maeda, A. Thomas, K. Takanebe, G. Xin, J. M. Carlsson, K. Domen and M. Antonietti, *Nat. Mater.*, 2009, **8**, 76.
- 4 P. Niu, L. Zhang, G. Liu and H.-M. Cheng, *Adv. Funct. Mater.*, 2012, **22**, 4763.
- 5 K. Schwinghammer, B. Tuffy, M. B. Mesch, E. Wirnhier, C. Martineau, F. Taulelle, W. Schnick, J. Senker and B. V. Lotsch, *Angew. Chem. Int. Ed.*, 2013, **52**, 2435.
- 6 J. Yang, D. Wang, H. Han and C. Li, *Acc. Chem. Res.*, 2013, **46**, 1900.
- 7 K. Schwinghammer, M. B. Mesch, V. Duppel, C. Ziegler, J. Senker and B. V. Lotsch, *J. Am. Chem. Soc.*, 2014, **136**, 1730.
- 8 A. Kudo and Y. Miseki, *Chem. Soc. Rev.*, 2009, **38**, 253.
- 9 X. Chen, J. Zhang, X. Fu, M. Antonietti and X. Wang, *J. Am. Chem. Soc.*, 2009, **131**, 11658.
- 10 X. Chen, S. Shen, L. Guo and S. S. Mao, *Chem. Rev.*, 2010, **110**, 6503.
- 11 S. Yang, Y. Gong, J. Zhang, L. Zhan, L. Ma, Z. Fang, R. Vajtai, X. Wang and P. M. Ajayan, *Adv. Mater.*, 2013, **25**, 2452.
- 12 Y. Zheng, J. Liu, J. Liang, M. Jaroniec and S. Z. Qiao, *Energy Environ. Sci.*, 2012, **5**, 6717.
- 13 S. Cao and J. Yu, *J. Phys. Chem. Lett.*, 2014, **5**, 2101.
- 14 L. Ge, C. Han, J. Liu and Y. Li, *Appl. Catal. A: Gen.*, 2011, **409-410**, 215.
- 15 C. Chang, Y. Fu, M. Hu, C. Wang, G. Shan and L. Zhu, *Appl. Catal. B: Environ.*, 2013, **142-143**, 553.
- 16 N. Cheng, J. Tian, Q. Liu, C. Ge, A. H. Qusti, A. M. Asiri, A. O. Al-Youbi and X. Sun, *ACS Appl. Mater. Interfaces*, 2013, **5**, 6815.
- 17 S. Tonda, S. Kumar, S. Kandula and V. Shanker, *J. Mater. Chem. A*, 2014, **2**, 6772.
- 18 X. Wang, X. Chen, A. Thomas, X. Fu and M. Antonietti, *Adv. Mater.*, 2009, **21**, 1609.
- 19 J. Xu, T. J. K. Brenner, Z. Chen, D. Neher, M. Antonietti and M. Shalom, *ACS Appl. Mater. Interfaces*, 2014, **6**, 16481.
- 20 S. C. Yan, Z. S. Li and Z. G. Zou, *Langmuir*, 2010, **26**, 3894.
- 21 J. Li, B. Shen, Z. Hong, B. Lin, B. Gao and Y. Chen, *Chem. Commun.*, 2012, **48**, 12017.
- 22 G. Liu, P. Niu, C. Sun, S. C. Smith, Z. Chen, G. Q. Lu and H.-M. Cheng, *J. Am. Chem. Soc.*, 2010, **132**, 11642.
- 23 J. Li, C. Cao and H. Zhu, *Nanotechnology*, 2007, **18**, 115605.
- 24 J. Liu, J. Huang, H. Zhou and M. Antonietti, *ACS Appl. Mater. Interfaces*, 2014, **6**, 8434.
- 25 W. Wang, J. C. Yu, Z. Shen, D. K. L. Chan and T. Gu, *Chem. Commun.*, 2014, **50**, 10148.
- 26 Q. Xiang, J. Yu and M. Jaroniec, *J. Phys. Chem. C*, 2011, **115**, 7355.
- 27 L. Ge and C. Han, *Appl. Catal. B: Environ.*, 2012, **117-118**, 268.
- 28 Z. Huang, F. Li, B. Chen, T. Lu, Y. Yuan and G. Yuan, *Appl. Catal. B: Environ.*, 2013, **136-137**, 269.
- 29 W. Wang, J. C. Yu, D. Xia, P. K. Wong and Y. Li, *Environ. Sci. Technol.*, 2013, **47**, 8724.
- 30 S. Kumar, T. Surendar, A. Baruah and V. Shanker, *J. Mater. Chem. A*, 2013, **1**, 5333.
- 31 X. Xu, G. Liu, C. Ransom and J. T. S. Irvine, *Int. J. Hydrogen Energy*, 2011, **36**, 13501.
- 32 L. Ge, C. Han and J. Liu, *Appl. Catal. B: Environ.*, 2011, **108-109**, 100.
- 33 Y. Wang, R. Shi, J. Lin and Y. Zhu, *Energy Environ. Sci.*, 2011, **4**, 2922.
- 34 Y. Hou, A. B. Laursen, J. Zhang, G. Zhang, Y. Zhu, X. Wang, S. Dahl and I. Chorkendorff, *Angew. Chem. Int. Ed.*, 2013, **52**, 3621.
- 35 Z. Zhao, Y. Sun and F. Dong, *Nanoscale*, 2015, **7**, 15.
- 36 Y. Zhang, H. Zhang, L. Cheng, Y. Miao, L. Hu, G. Ding and Z. Jiao, *Eur. J. Inorg. Chem.*, 2015, **2015**, 2895.
- 37 T. Xia, W. Zhang, J. B. Murowchick, G. Liu and X. Chen, *Adv. Energy Mater.*, 2013, **3**, 1516.
- 38 X. Chen, L. Liu, P. Y. Yu and S. S. Mao, *Science*, 2011, **331**, 746.
- 39 J. Jun, M. Dhayal, J.-H. Shin, J.-C. Kim and N. Getoff, *Radiat. Phys. Chem.*, 2006, **75**, 583.
- 40 M. M. Khan, S. A. Ansari, D. Pradhan, M. O. Ansari, D. H. Han, J. Lee and M. H. Cho, *J. Mater. Chem. A*, 2014, **2**, 637.
- 41 Y. Zhang, J. Liu, G. Wu and W. Chen, *Nanoscale*, 2012, **4**, 5300.
- 42 S. C. Yan, Z. S. Li and Z. G. Zou, *Langmuir*, 2009, **25**, 10397.
- 43 Y.-P. Yuan, L.-S. Yin, S.-W. Cao, L.-N. Gu, G.-S. Xu, P. Du, Y. Chai, Y.-S. Liao and C. Xue, *Green Chem.*, 2014, **16**, 4663.
- 44 J. Xu, Y. Wang and Y. Zhu, *Langmuir*, 2013, **29**, 10566.
- 45 X. Bai, L. Wang, R. Zong and Y. Zhu, *J. Phys. Chem. C*, 2013, **117**, 9952.
- 46 F. Yang, V. Kuznetsov, M. Lublow, C. Merschjann, A. Steiger, T. Klaer, A. Thomas and T. Schedel-Niedrig, *J. Mater. Chem. A*, 2014, **2**, 6407.
- 47 Y. Zhang, Q. Pan, G. Chai, M. Liang, G. Dong, Q. Zhang and J. Qiu, *Sci. Rep.*, 2013, **3**, 1943.
- 48 X. L. Wang, W. Q. Fang, H. F. Wang, H. Zhang, H. Zhao, Y. Yao and H. G. Yang, *J. Mater. Chem. A*, 2013, **1**, 14089.

- 49 Y. Shiraishi, S. Kanazawa, Y. Sugano, D. Tsukamoto, H. Sakamoto, S. Ichikawa and T. Hirai, *ACS Catal.*, 2014, **4**, 774.
- 50 Y. Chen, J. Li, Z. Hong, B. Shen, B. Lin and B. Gao, *Phys. Chem. Chem. Phys.*, 2014, **16**, 8106.
- 51 D. J. Martin, K. Qiu, S. A. Shevlin, A. D. Handoko, X. Chen, Z. Guo and J. Tang, *Angew. Chem. Int. Ed.*, 2014, **53**, 9240.
- 52 E. Kroke, M. Schwarz, E. Horath-Bordon, P. Kroll, B. Noll and A. D. Norman, *New J. Chem.*, 2002, **26**, 508.
- 53 L. Ming, H. Yue, L. Xu and F. Chen, *J. Mater. Chem. A*, 2014, **2**, 19145.

Fig. 1 TEM (a) and SEM (b) images of typical $g\text{-C}_3\text{N}_4$.

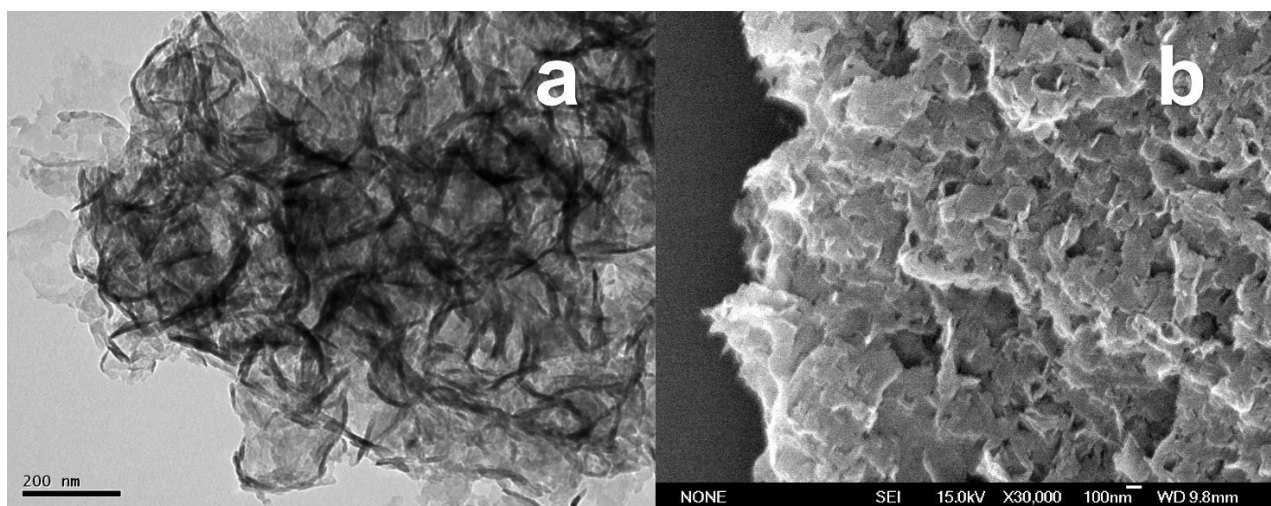


Fig. 2 Optical photographs of $g\text{-C}_3\text{N}_4$ with different post-treatments (a) and corresponding fluorescence phenomenon under UV excitation (b).

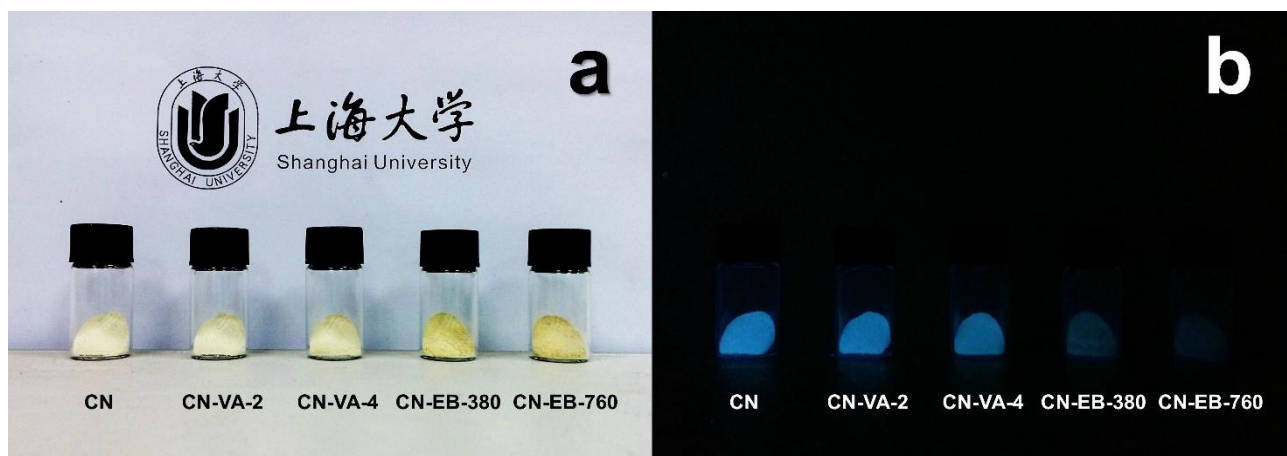


Fig. 3 XRD patterns of CN, CN-VA-2, CN-VA-4, CN-EB-380 and CN-EB-760.

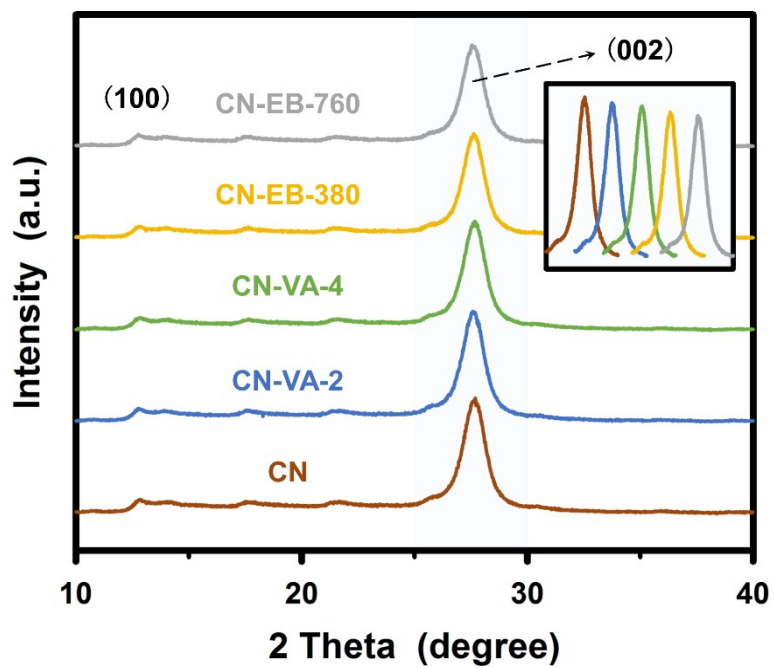


Fig. 4 FT-IR (a) and Raman (b) spectra of CN, CN-VA-2, CN-VA-4, CN-EB-380 and CN-EB-760.

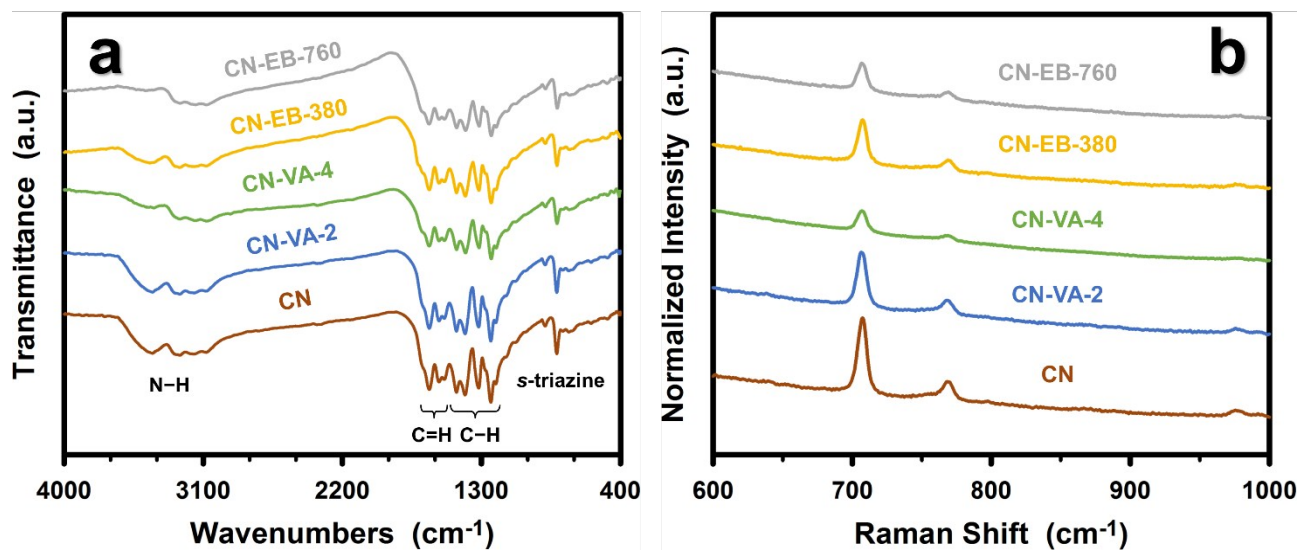


Fig. 5 UV-Vis DR (a), PL (c) spectra of $g\text{-C}_3\text{N}_4$ with different post-treatments and corresponding plots of Kubelka-Munk function versus the energy of light (b); $F(R) = (1-R)^2 \cdot (2R)^{-1} = K \cdot S^{-1}$, where R, K and S were reflectance, effective absorption and scattering coefficients, respectively.

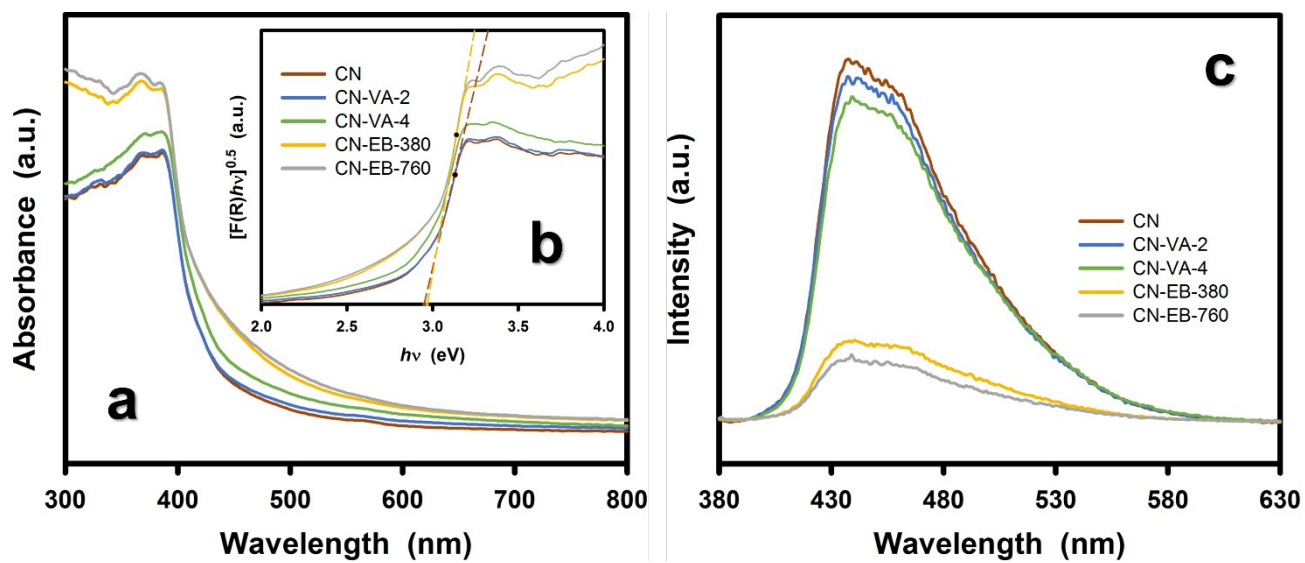


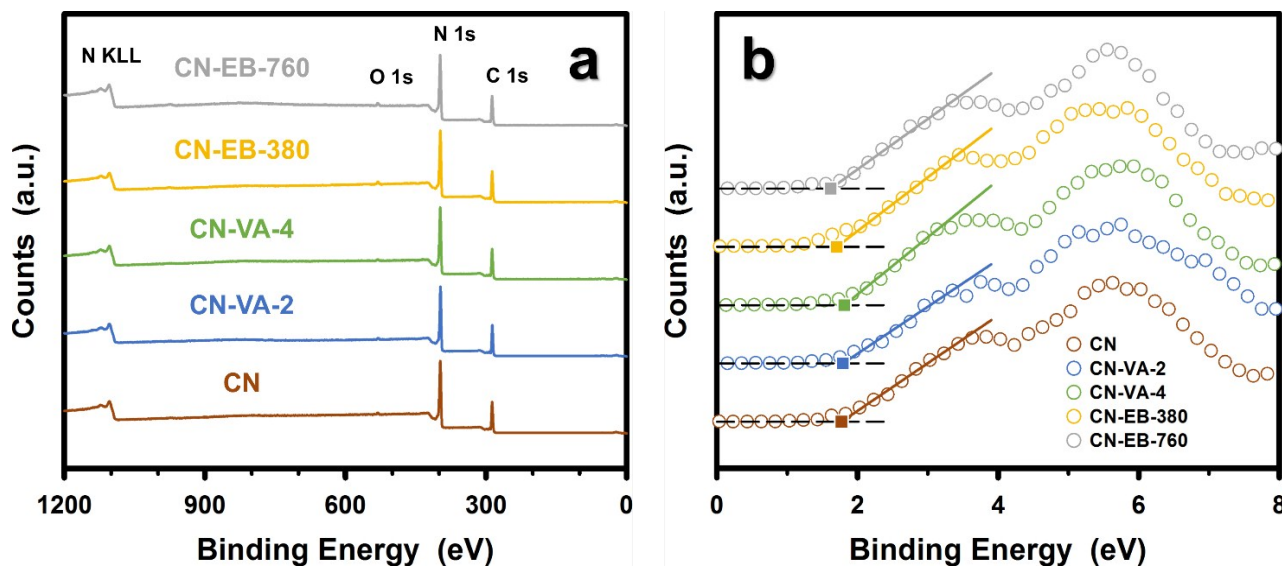
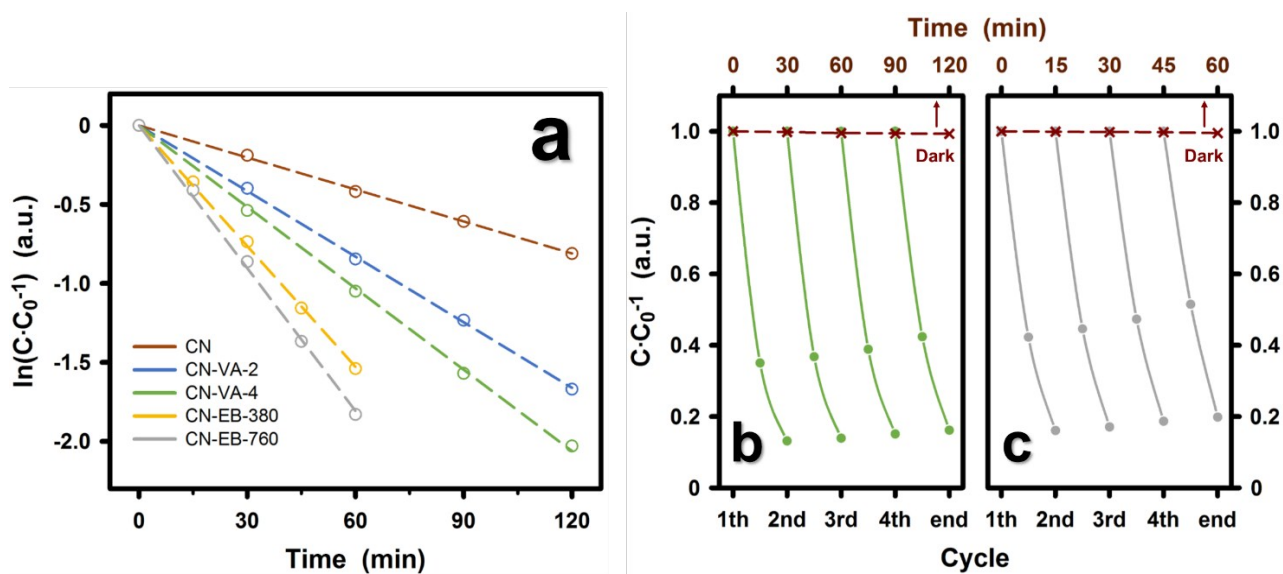
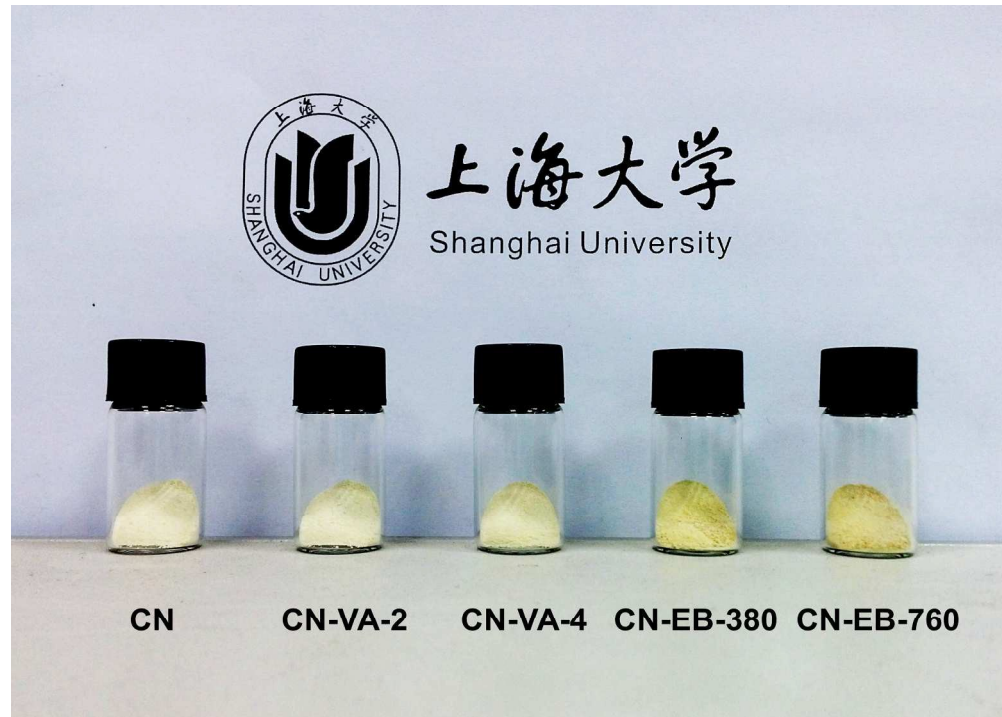
Fig. 6 XPS survey (a) and VB (b) spectra of CN, CN-VA-2, CN-VA-4, CN-EB-380 and CN-EB-760.

Table I Ratios of bonds within the N 1s core-level peak in different samples and corresponding VBM energies.

	C–N–C (%)	N–[C] ₃ (%)	C–NH _x (%)	VBM (eV)
CN	71.1	22.6	6.3	1.77
CN-VA-2	70.8	22.8	6.4	1.79
CN-VA-4	71.2	22.6	6.2	1.81
CN-EB-380	67.3	26.2	6.5	1.70
CN-EB-760	68.0	25.8	6.2	1.62

Fig. 7 Photocatalytic degradation of RhB in the presence of CN, CN-VA-2, CN-VA-4, CN-EB-380 and CN-EB-760 (a). Cycle and dark control degradation of RhB in the presence of CN-VA-4 (b) and CN-EB-760 (c).





694x496mm (96 x 96 DPI)